Flame and Soot Boundaries of Laminar Jet Diffusion Flames

F. Xu,* Z. Dai,† and G. M. Faeth‡
University of Michigan, Ann Arbor, Michigan 48109-2140

The shapes (flame-sheet and luminous-flame boundaries) of steady weakly buoyant round hydrocarbon-fueled laminar-jet diffusion flames in still and coflowing air were studied both experimentally and theoretically. Flame-sheet shapes were measured from photographs using a CH optical filter to distinguish flame-sheet boundaries in the presence of blue CO_2 and OH emissions and yellow continuum radiation from soot. Present experimental conditions included acetylene-, methane-, propane-, and ethylene-fueled flames having initial reactant temperatures of 300 K, ambient pressures of 4–50 kPa, jet-exit Reynolds numbers of 3–54, initial air/fuel velocity ratios of 0–9, and luminous flame lengths of 5–55 mm; earlier measurements for propylene- and 1,3-butadiene-fueled flames for similar conditions were considered as well. Nonbuoyant flames in still air were observed at microgravity conditions; essentially nonbuoyant flames in coflowing air were observed at small pressures to control effects of buoyancy. Predictions of luminous flame boundaries from soot luminosity were limited to laminar smoke-point conditions, whereas predictions of flame-sheet boundaries ranged from soot-free to smoke-point conditions. Flame-shape predictions were based on simplified analyses using the boundary-layer approximations along with empirical parameters to distinguish flame-sheet and luminous-flame (at the laminar smoke point) boundaries. The comparison between measurements and predictions was remarkably good and showed that both flame-sheet and luminous-flame lengths are primarily controlled by fuel flow rates with lengths in coflowing air approaching $\frac{2}{3}$ of the lengths in still air as coflowing air velocities are increased. Finally, luminous flame lengths at laminar smoke-point conditions were roughly twice as long as flame-sheet lengths at comparable conditions because of the presence of luminous soot particles in the fuel-lean region of the flames.

Nomenclature

C_f	=	empirical soot factor
C_n	=	empirical coflow factor
D	=	mass diffusivity
d	=	jet-exit diameter
Fr_a, Fr_f	=	air- and fuel-stream Froude numbers, $u_{ao}^2/(2gL_f)$ and $u_{fo}^2/(2gL_f)$
g	=	acceleration of gravity
L_f	=	distance from jet exit to either flame-sheet or luminous-flame tip
L_o	=	distance from jet exit to virtual origin
$\dot{m}$	=	burner mass flow rate
$\dot{m}_f$	=	burner fuel mass flow rate
p	=	pressure
Re	=	jet Reynolds number, $4\dot{m}/(\pi d\mu)$
r	=	radial distance
Sc	=	Schmidt number, ν/D
u	=	streamwise velocity
w	=	luminous flame diameter
$w_{1/2}$	=	luminous flame diameter at $\zeta = \frac{1}{2}$
x	=	streamwise distance
Z_{st}	=	stoichiometric mixture fraction
ζ	=	normalized streamwise distance; Eq. (4)
μ	=	dynamic viscosity
ν	=	kinematic viscosity

Subscripts

a	=	airstream property
f	=	fuel-stream property
MAX	=	maximum value
o	=	burner exit plane or virtual origin condition

Introduction

LAMINAR nonpremixed (diffusion) flames are of interest because they provide model flame systems that are far more tractable for analysis and experiments than practical turbulent diffusion flames. Clearly, an understanding of laminar diffusion flames must precede an understanding of more complex turbulent diffusion flames. In addition, many properties of laminar diffusion flames are directly relevant to turbulent diffusion flames using laminar flamelet concepts. Finally, laminar diffusion flame shapes have been of interest since the classical study of Burke and Schumann[1] because they involve a simple nonintrusive measurement that is convenient for evaluating flame structure predictions. Motivated by these observations, the shapes of round laminar-jet diffusion flames were considered both experimentally and theoretically during the present investigation. The study was limited to flames where effects of buoyancy were either nonexistent or small, however, in order to minimize parameters and because most practical flames are not buoyant.

Most earlier studies of the shapes of hydrocarbon-fueled nonbuoyant laminar-jet diffusion flames have considered combustion in still air (see Refs. 2–6 and references cited therein). These studies have shown that soot-containing flames at the laminar smoke point (flames at the condition of onset of soot emissions) have luminous flame lengths roughly twice as long as the length of flame sheet (the position where fuel and oxidant combine in roughly stoichiometric proportions generally within a thin reaction zone) and have developed simple but effective ways to estimate their shapes.[4,5] Corresponding studies of hydrocarbon-fueled nearly nonbuoyant (weakly buoyant) laminar-jet diffusion flames burning in coflowing air have also been reported (see Refs. 1, 7–9, and references cited therein). These studies were limited to soot-containing flames at laminar smoke-point conditions and also developed simple but effective ways to estimate their shapes; however, the corresponding behavior of the flame sheet for these conditions [in either soot-free

(blue) flames or soot-containing flames] has not been addressed. This is unfortunate because hydrodynamic effects to reduce soot concentrations in diffusion flames are of great interest.[10–19] In addition, soot-free hydrocarbon-fueled flames are fundamentally important because they have enhanced computational tractability compared to soot-containing flames as a result of the absence of the complexities of soot chemistry, and they provide results useful for evaluating detailed models of hydrocarbon-fueled flame chemistry and transport.

The ability to achieve soot-free laminar diffusion flames by subjecting the fuel stream to higher momentum (velocity) oxidant streams (e.g., by strong coflows), similar to the behavior of air atomization processes,[11,18,19] is discussed by Lin and Faeth[18] and Dai and Faeth.[19] The effect of enhanced coflow comes about because the position of the flame sheet tends to be fixed by the fuel flow rate independent of the coflow velocity at large coflow velocities,[9] which implies that characteristic residence times for soot formation are inversely proportional to the coflow velocity.[18,19] Thus, increasing the coflow velocity inhibits soot emissions and eventually leads to completely soot-free (blue) flames as long as flame liftoff conditions are not exceeded. This tactic was exploited during the present study in order to provide conditions where the shapes of the flame sheet of hydrocarbon-fueled laminar-jet diffusion flames in coflowing air could be observed.

Thus, the objectives of the present investigation were to observe the flame-sheet shapes of weakly buoyant laminar-jet diffusion flames in coflowing air considering both soot-free and soot-containing flames and to use these results to develop a simplified model of flame-sheet shape for these conditions. Corresponding results for laminar-jet diffusion flames in nearly still air are also considered in order to highlight effects of coflow on flame structure, soot formation, and soot emission properties. Finally, luminous flame shapes at the laminar smoke point, in both still and coflowing air, are also considered for completeness, exploiting earlier measurements in the literature.[5,9]

Experimental Methods

Test Apparatus

Experimental methods were similar to Lin et al.,[5] Lin and Faeth,[9] and Lin[17] and will be described only briefly. Effects of buoyancy were minimized by observing flames at relatively small pressures (≤ 50 kPa) with either relatively large coflow velocities (air/fuel velocity ratios up to nine) or with relatively large source fuel Froude numbers when coflow velocities were small. The burner was placed within a windowed cylindrical chamber and directed vertically upward along the chamber axis. The windowed chamber had a diameter of 300 mm and a length of 1200 mm. Optical access was provided by two pairs of opposing windows having diameters of 100 mm and centered on a horizontal plane located 500 mm above the base of the windowed chamber. The flames were positioned so that their full lengths could be observed and photographed through the windows.

The burner was a coaxial-tube arrangement with the fuel flowing from the inner port (1.6-, 3.2-, and 4.8-mm inside diameters with the outer wall of the tube tapered to provide a negligible thickness at the tube exit) and air flowing from a concentric outer port (60-mm inside

diameter). The inner port had sufficient length to provide fully developed laminar pipe flow at the burner exit. The outer port had several layers of beads and screens to provide a uniform nonturbulent flow at the burner exit. Flame lengths were limited so that test conditions approximated flames in a uniform air coflow based on earlier laser velocimetry measurements of flow velocity distributions.[17,18] The burner tube exit was placed 10 mm above the last screen of the air coflow so that the flames were free to attach somewhat below the burner exit (which often was the case unless liftoff conditions were approached).

Fuel was supplied to the inside port from commercial gas cylinders. Fuel flow rates were controlled and metered using critical flow orifices in conjunction with pressure regulators; the flow properties of the orifices were calibrated using wet-test meters. Air was supplied from the room using critical-flow orifices to control and meter airflow rates. The exhaust products were diluted with air to reduce flow temperatures and then removed using the laboratory vacuum pump system. The flames were ignited using a small torch that was removed from the flowfield after the flames had stabilized.

Instrumentation

Dark-field photographs of the flames were obtained using a 35-mm reflex camera. The photographs were subsequently printed using a 100×125 mm film format and then scanned. Flame shapes were measured directly from the scanned images, using objects of known size to calibrate vertical and horizontal distances. Experimental uncertainties (95% confidence) of luminous flame diameters and lengths were less than 2%.

The dark-field color photographs sufficed to locate luminous-flame boundaries as either the outer extremity of yellow luminosity caused by continuum radiation from soot or the inner boundary of blue luminosity from the flame sheet (which exhibited a significant afterglow of OH luminosity for the low-pressure flames observed during the present experiments). To locate the flame sheet, however, dark-field photographs were obtained using a narrowband filter designed to pass radiation from the excited CH band associated with radical reactions at the flame sheet (430-nm center frequency with a 10-nm half-width pass band). This luminosity was relatively weak, but the present flames were very steady so that exposure times could be increased to obtain satisfactory photographs. The outer extremity of the CH image was taken as the flame-sheet location because CH luminosity is not associated with fuel-lean regions of the present flames. Experimental uncertainties of the flame-sheet measurements are the same as the luminous flame boundary measurements.

Test Conditions

Test conditions are summarized in Table 1. Present measurements considered methane-, acetylene-, ethylene-, and propane-fueled flames; earlier measurements considered propylene- and 1,3-butadiene-fueled flames. Gas purities were greater than 99% by volume for all of the fuel gases except acetylene, which only had a 98% purity by volume, because of contamination by acetone, which is present in commercial acetylene gas cylinders for safety purposes. The effect of acetone on the properties of flames similar to the present flames was evaluated during earlier experiments.[17,18]

Table 1 Summary of test conditions[a]

Parameter[b]	CH_4	C_2H_2	C_2H_4	C_3H_6	C_3H_8	C_4H_6
Fuel flow rate, mg/s	0.49–3.12	0.41–4.88	0.50–4.66	1.53–4.08	0.59–3.81	0.74–2.71
Re	2.7–45.6	2.9–54.1	3.6–47.6	38–101	4.9–48.5	18–66
u_{ao}/u_{fo}	0.008–7.14	0.0058–5.01	0.009–8.80	0.3–7.0	0.012–5.71	0.8–32.5
p, kPa	21.3–49.4	4.1–21.3	8.5–21.5	19–50	11.3–35.2	19–50
d, mm	1.6, 4.8	1.6, 4.8	1.6, 4.8	4.8	1.6, 4.8	4.8
μ_{fo}, mg/s-m	48.0	51.7	49.7	49.3	47.0	49.8
L_f, mm	5.7–41.5	5.0–54.9	7.1–47.0	41–108	9.4–51.3	21–75
$w_{1/2}$, mm	6.5–17.7	7.9–24.4	7.9–24.7	5.9–13.1	8.1–22.4	4.3–10.0
Z_{st}	0.0552	0.0704	0.0638	0.0636	0.0603	0.0668

[a]Air port inside diameter of 60 mm with burner directed vertically upward. Reactant temperatures of roughly 300 K.
[b]Commercial gases in cylinders with purities as follows: greater than 98.0% by volume for C_2H_2 and greater than 99.0% by volume for the rest.

This was done by comparing observations with and without acetone vapor present, using the acetone removal system described by Hamins et al.[20] to create an acetone-free acetylene fuel stream. The effect of acetone on luminous flame shapes and laminar smoke-point flame lengths was found to be small.[17,18]

Theoretical Methods

Flame-shape predictions were obtained using the simplified analysis of Lin et al.[5] for laminar diffusion flames in still air and Lin and Faeth[9] for laminar diffusion flames in coflowing air. In both instances a set of easily used equations was sought, along with recommendations for selecting the thermochemical and transport properties appearing in the equations, rather than more complete methods that would require numerical solution using a computer. The approach used for flames in still gases was to extend the analysis of Spalding,[2] which is described in more detail by Kuo,[3] as discussed by Lin et al.[5]; the approach used for flames in coflowing gases was to extend the analysis of Mahalingam et al.,[8] as discussed by Lin and Faeth.[9]

Except for ambient flow properties, the major assumptions of flame-shape analyses in still and coflowing gases were the same,[9] as follows: 1) steady, axisymmetric laminar-jet diffusion flames at constant pressure in an unbounded environment having uniform properties (velocities and scalar properties); 2) effects of buoyancy and associated changes of potential energy are negligible; 3) flow Mach numbers are small so that effects of kinetic energy and viscous dissipation are negligible; 4) the flames have large aspect ratios so that diffusion of mass (species), momentum, and energy in the streamwise direction is small; 5) for the same reasons the solution of the governing equations can be approximated by far-field conditions where the details of the initial conditions can be replaced by integral invariants of the flow for the conservation of mass, momentum, and energy; 6) similarly, the convection velocities of the flow can be approximated by ambient streamwise velocities for the coflow case; 7) all chemical reactions occur within a thin-flame sheet with fast chemistry so that fuel and oxidant are never simultaneously present at finite concentrations; 8) the diffusivities of mass (of all species), momentum, and energy are all equal; 9) all thermophysical and transport properties are constant throughout the flame; and 10) effects of radiation are small. The first three assumptions are justified as conditions of the present experiments. The fourth and fifth assumptions are justified for most of the present measurements because the present flames generally had large aspect ratios, for example, some measurements involve $(L_f - L_o)/d$ as small as 1.0 but most of the measurements involve $(L_f - L_o)/d$ in the range 6–22. The sixth assumption is widely used to approximate wake-like boundary-layer flows at large aspect ratios.[9] The seventh assumption, prescribing a thin flame sheet, has a long history of effective use to find the shapes of laminar diffusion flames, dating back to Burke and Schumann.[1] The remaining assumptions are not satisfied by laminar-jet diffusion flames, however, and are only adopted so that simple flame-shape formulas can be found based on the past success of similar approximations to find the shapes of the luminous soot boundaries of laminar-jet diffusion flames at the laminar smoke point (see Refs. 5 and 9 and references cited therein).

Under these assumptions a simple formula can be obtained for flame-sheet and luminous-flame lengths both in still and strongly coflowing gases, as follows[9]:

$$(L_f - L_o)/d = C_f C_n Re\,Sc/Z_{st} \tag{1}$$

where $C_n = \frac{3}{32}$ and $\frac{2}{32}$ for weak and strong coflow and C_f is roughly 0.5 and 1.0 for the flame-sheet location and for the location of the luminous-flame boundary at laminar smoke-point conditions, respectively. (More accurate selections of C_f will be considered later.) The algorithm for computing flame properties from Eq. (1) was completed by using the values for the Schmidt number and the viscosity of air at the average of the adiabatic flame temperature and the ambient temperature from Braun et al.[21] Typical of past work with hydrocarbon-fueled laminar-jet diffusion flames burning in air, the value of the Schmidt number did not change significantly over the test range; thus, $Sc = 0.76$ was used for all of the results considered during the present investigation. Similarly, the correlations of flame lengths were improved during past work by introducing the empirical virtual origin parameter L_o/d (see Refs. 5 and 9). The effect of a virtual origin was not very significant for present conditions, however, so that $L_o/d = 0$ was used instead.

The expressions for luminous-flame diameters differ for laminar-jet diffusion flames in still air, given in Ref. 5, and in coflowing air, given in Ref. 9. For flames in still air, the expression becomes[5]

$$wZ_{st}/d = 3^{\frac{1}{2}}\zeta\left(\zeta^{-\frac{1}{2}} - 1\right)^{\frac{1}{2}} \tag{2}$$

whereas the corresponding equation for flames in coflowing air becomes[9]

$$wZ_{st}/d = [-\zeta(u_{fo}/u_{ao})Z_{st}\ell n\{\zeta\}]^{\frac{1}{2}} \tag{3}$$

And in both cases

$$\zeta = (x - L_o)/(L_f - L_o) \tag{4}$$

and the values of the flame diameter at the midposition of the flames, where $\zeta = \frac{1}{2}$, are given as follows for flames in still air[5]:

$$w_{\frac{1}{2}}Z_{st}/d = 0.557 \tag{5}$$

whereas the corresponding equation for flames in coflowing air becomes[9]

$$w_{\frac{1}{2}}Z_{st}/d = [Z_{st}(u_{fo}/u_{ao})\,\ell n\{2\}/2]^{\frac{1}{2}} \tag{6}$$

Other expressions for the maximum value of w, w_{MAX}, can be found in Refs. 5 and 9, but the differences between $w_{1/2}$ and w_{MAX} are not large.

Results and Discussion

Flame Appearance

Photographs of a soot-free acetylene-fueled laminar-jet diffusion flame in coflowing air at near liftoff conditions are illustrated in Fig. 1. The figure on the left is a black-and-white image of a conventional dark-field color photograph. The figure at the right is a black-and-white image of a dark-field color photograph obtained using the CH filter. Both images are essentially the same indicating that the flame sheet in the absence of soot luminosity is indicated equally well by conventional dark-field color photographs as well as the image obtained from CH luminosity alone.
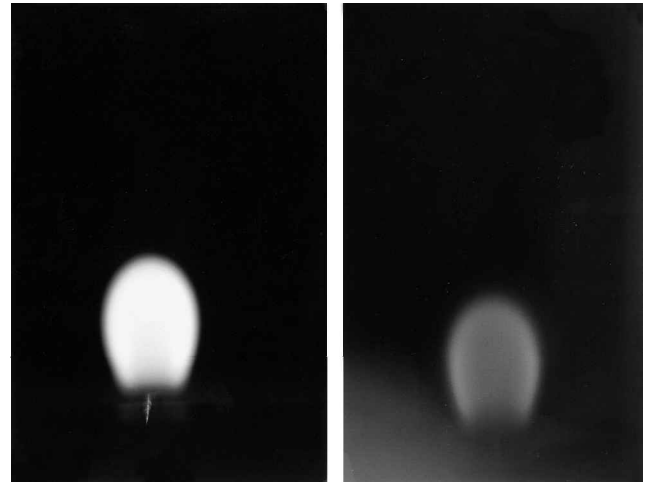

Fig. 1 Photographs of a soot-free acetylene-fueled laminar-jet diffusion flame burning in coflowing air near the liftoff condition, without (left) and with (right) the C-H filter. Test conditions are $d = 1.6$ mm, $p = 4.1$ kPa, and $u_{ao}/u_{fo} = 0.05$.
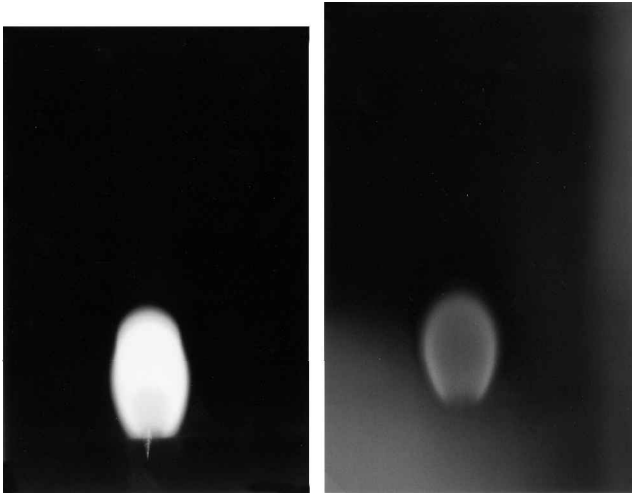
Fig. 2 Photographs of a soot-containing acetylene-fueled laminar-jet diffusion flame burning in coflowing air at conditions between laminar soot and smoke points, without (left) and with (right) the C-H filter. Test conditions are $d = 1.6$ mm, $p = 8.2$ kPa, and $u_{ao}/u_{fo} = 0.06$.

Photographs of a soot-containing acetylene-fueled laminar-jet diffusion flame in coflowing air are illustrated in Fig. 2 for conditions intermediate between the laminar soot and smoke points. Similar to Fig. 1, the figure on the left is a black-and-white image of a conventional dark-field color photograph, whereas the figure at the right is a black-and-white image of a dark-field color photograph obtained using the CH filter. In this case the conventional color photograph image is longer than the color images obtained using the CH filter because of the presence of yellow luminosity from hot soot particles present beyond the flame-sheet in the fuel-lean region of the flame. (This is more evident based on direct viewing of the flame by eye or from the conventional color image where the yellow color can be seen.) Similar to Fig. 1, however, both images are identical near the burner exit where no soot was present. Thus, it was possible to locate the image of the flame sheet using the CH filter even in the presence of significant soot luminosity from the fuel-lean portion of the flame once the laminar soot-point condition was exceeded.

Flame Lengths

Luminous-flame lengths are defined in the following as the streamwise distance between the burner exit and the farthest downstream plane normal to the flame axis that contacts a luminous region of the flame, at the laminar smoke point, similar to Lin and Faeth.[9] For flames in coflowing air, this length was associated with the end of the flame luminosity at the flame axis. For the flames of Lin et al.[5] in still air, however, this location was either along the axis or at an annular soot layer for the closed- and open-tip flames observed near laminar smoke-point conditions for nonbuoyant flames in still gases.[6] This distinction was not necessary for flame-sheet lengths, however, because this length was always associated with the end of flame luminosity at the flame axis, as observed either using the CH filter for soot-containing flames or observed both with and without the CH filter for soot-free flames.

For present conditions, only fuel flowed from the fuel port so that simple one-dimensional conservation of mass principles apply, and an expression for flame length as a function of the fuel flow rate can be obtained from Eq. (1) and the definition of the Reynolds number, as follows:

$$L_f - L_o = 4C_f C_n Sc\, \dot{m}_f / (\pi Z_{st} \mu) \qquad (7)$$

Noting that $L_o \ll L_f$ from Table 2, Eq. (7) implies that both the flame-sheet length (at the axis) and the luminous-flame length (at the laminar smoke point) are proportional to the parameter $\dot{m}_f / (Z_{st} \mu)$ because C_f, C_n, and Sc are not affected by either fuel type or the value of $\dot{m}_f / (Z_{st} \mu)$ for present conditions. Similar behavior concerning relationships between fuel flow rates and laminar

Table 2   Summary of flame-length correlations[a]

Flame system	Source	L_o/d	C_f	C_n
Smoke-point flame length in still air, $Fr_f = \infty$	Lin et al.[5]	−3.2	1.13	$\frac{3}{32}$
Smoke-point flame length in coflowing air; $u_{ao}/u_{fo} > 1$ and $Fr_a > 1$	Lin and Faeth[9]	1.4	1.05	$\frac{2}{32}$
Soot-free flame length in still air; $u_{ao}/u_{fo} < 0.2$ and $Fr_f \gg 5$	Present study	0.0	0.52	$\frac{3}{32}$
Soot-free flame length in still air; $u_{ao}/u_{fo} = 0$ and $Fr_f = \infty$	Sunderland et al.[4]	2.7	0.56	$\frac{3}{32}$
Soot-free flame length in coflow; $u_{ao}/u_{fo} > 0.5$ and $Fr_a > 1$	Present study	0.0	0.54	$\frac{2}{32}$

[a]Empirical flame length parameters based on Eq. (1) for soot-free flames and for soot-containing flames at the laminar smoke point for flames in still ($u_{ao}/u_{fo} < 0.2$) or coflowing ($u_{ao}/u_{fo} > 0.5$) air.
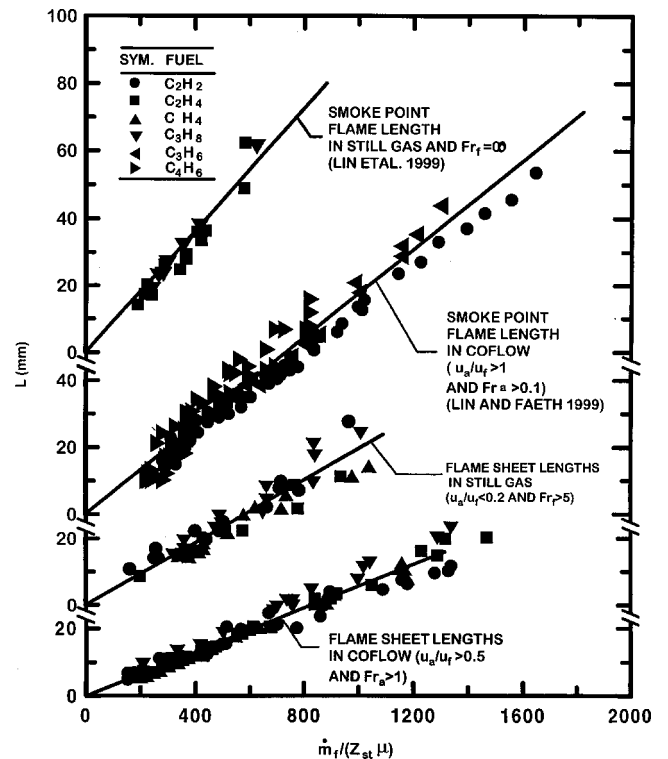

Fig. 3   Flame-sheet and luminous-flame lengths (the latter at the laminar smoke point) of laminar-jet diffusion flames in still air and coflowing air. Measurements from Lin et al.,[5] Lin and Faeth,[9] and the present investigation.

smoke-point flame lengths for buoyant flames has been recognized for some time[14,22,23] and has also been observed for nonbuoyant flames at the laminar smoke point as suggested by Eq. (5).[24,25]

Measured flame-sheet and luminous-flame lengths (the latter at the laminar smoke-point condition) are plotted according to Eq. (7) in Fig. 3 for nonbuoyant diffusion flames in both nearly still and relatively strong coflowing air. The values of C_f and C_n for the correlations were taken from Table 2, whereas $Sc = 0.76$ for all of the present results as noted earlier. Thus, Eq. (7) combined with present methods of finding flame physical properties and the values of C_f and C_n from Table 2 yield excellent correlations for the four flame length conditions that are considered in Fig. 3. The measured flame-sheet results include conditions in both soot-free (blue) flames as well as conditions beyond the laminar soot point (but prior to the laminar smoke point) where soot is present and the flame exhibits yellow soot luminosity. Similar to the discussion of Fig. 2, however,

the presence of soot in the present laminar-jet diffusion flames did not have a significant effect on the flame-sheet length. The values of C_f at the luminous-flame length at the laminar smoke-point condition are roughly twice as large as the values of C_f for the flame-sheet length (see Table 2); thus, the presence of hot soot particles in the fuel-lean portion of the flame significantly extends (by up to a factor of roughly 2) the region where flame luminosity is observed.

The measurements illustrated in Fig. 3 could be grouped into conditions where $u_a/u_f > 0.5$ and the various lengths correlated reasonably well with the coflow correlation with $C_n = \frac{2}{32}$ (as long as $Fr_a > 1$) and $u_{ao}/u_{fo} < 0.2$ where the various lengths correlated reasonably well with the still gas correlation with $C_n = \frac{3}{32}$ (as long as $Fr_f > 5$). Intermediate values of u_{ao}/u_{fo} yield intermediate values of flame lengths (or C_n) as will be discussed in more detail later. In view of the simplicity of the theory, it is remarkable that the predictions are reasonably good. Thus, transition from strong to weak coflow increases both flame-sheet and luminous-flame lengths by roughly 50%. The reason that values of u_{ao}/u_{fo} are significantly less than unity bound conditions between strong and weak coflow is that jet-exit conditions decay rapidly toward ambient conditions so that even relatively small ambient velocities can affect mixing in the important region near the flame tip for flame length behavior, particularly for the relatively large aspect ratio flames (typical of the behavior of hydrocarbon/air flames that have relatively small stoichiometric ratios or small values of Z_{st}) that were considered during the present investigation.

Flame Diameters

It is evident that the normalized characteristic flame diameter $w_{1/2}Z_{st}/d$ for laminar-jet diffusion flames is a constant for flames in still air from Eq. (2) and is inversely proportional to the square root of air/fuel velocity ratio for flames in coflowing air from Eq. (3), independent of flow transport properties. This relationship is illustrated in Fig. 4 for nonbuoyant diffusion flames in coflow for flame-sheet diameters with $u_{ao}/u_{fo} > 0.5$ and $Fr_a > 1$ along with the predictions of Eq. (3). The measurements scatter about the predictions, but the scatter progressively decreases as the normalized flame length increases. Thus, small flame aspect ratios appear to be mainly responsible for the scatter seen in Fig. 4. This conclusion is similar to the findings of Lin and Faeth[9] for laminar smoke-point conditions.

It is also of interest to consider the behavior of the normalized characteristic flame diameter as the value of u_{ao}/u_{fo} increases for conditions representative of nonbuoyant laminar-jet diffusion

Fig. 5 Measured and predicted flame-sheet diameters as a function of air/fuel velocity ratios.

flames in still air to strongly coflowing air. This transition is considered in Fig. 5, which provides characteristic flame diameter expressions particularly suitable for both large and small values of u_{ao}/u_{fo}. Results illustrated in Fig. 5 show the transition between estimates of the characteristic flame diameter in still gas to estimates in strongly coflowing gas at values of $u_{ao}/u_{fo} \approx 0.1$; measured results in both regimes exhibit significant degrees of scatter, and the large coflow predictions generally underestimate the measurements.

Flame Shapes

Measured and predicted flame shapes will be compared as the final step in the evaluation of the simplified flame-shape analyses leading to Eqs. (1–4) for nonbuoyant laminar-jet diffusion flames in still and coflowing air. These evaluations will consider a range of flame aspect ratios in order to explore the robustness of the predictions. Both soot-free and soot-containing flames will be considered in the following so that effects of soot on the location of the flame sheet can be evaluated for nonbuoyant laminar-jet diffusion flames.

Examples of measured and predicted flame shapes for soot-free methane/air flames having various coflow velocity ratios are illustrated in Fig. 6. For these soot-free flame conditions the measured flame shapes with and without the CH filter are identical, with both observations giving the correct flame-sheet location. Predictions of flame-sheet locations using the simplified theories are also shown on the plot; all of the measurements are for $u_{ao}/u_{fo} > 0.5$ and are compared with predictions for flames in coflowing air, Eq. (3). The comparison between measurements and predictions is excellent, properly accounting for effects of variations of air coflow, in view of the simplicity of the flame-shape analyses.

Examples of measured and predicted flame-sheet shapes for soot-containing ethylene/air flames having various coflow velocity ratios are illustrated in Fig. 7. For these soot-containing flame conditions measured flame shapes with and without the CH filter are no longer identical with the luminous-flame shape obtained without the filter extending farther downstream as a result of the presence of yellow soot luminosity from soot present in the fuel-lean region of the flame. None of the conditions shown in Fig. 7 correspond to laminar smoke-point conditions; therefore, only laminar flame-sheet predictions are shown on the plot. Similar to Fig. 6 for soot-free flames, the comparison between measurements and predictions is excellent, indicating that the presence of soot in these flames
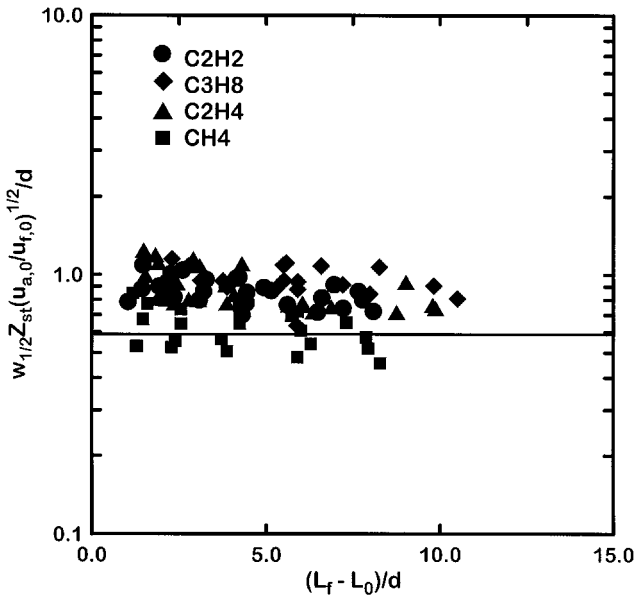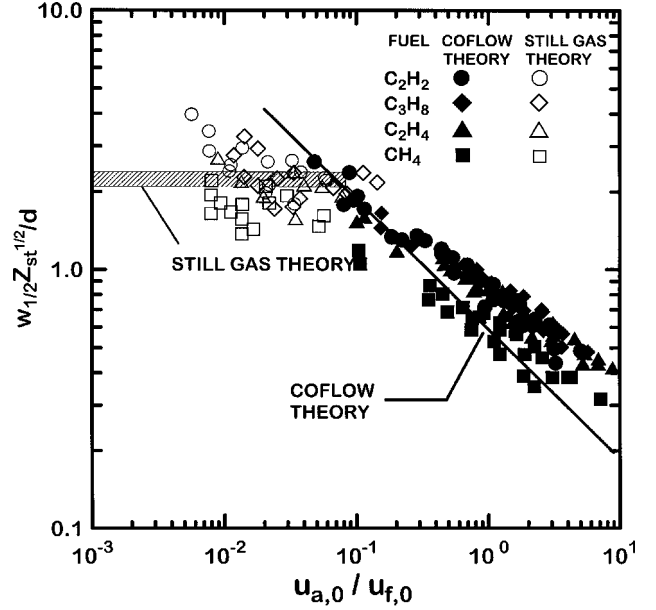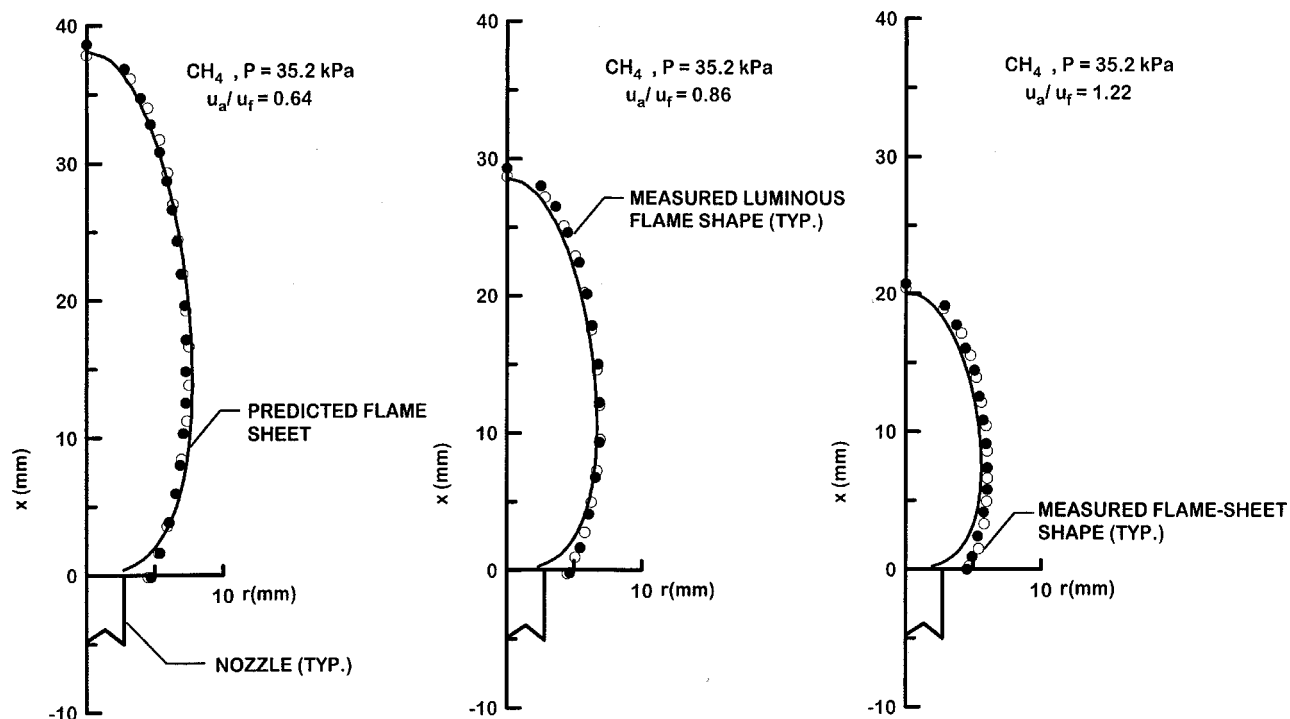

Fig. 4 Measured and predicted flame-sheet diameters for laminar-jet diffusion flames in coflow as a function of air/fuel velocity ratios and flame sheet length.

Fig. 6 Measured flame-sheet and luminous-flame shapes and predicted flame-sheet shapes for soot-free methane-fueled laminar-jet diffusion flames having a burner diameter of 4.8 mm at various air coflow velocity ratios.
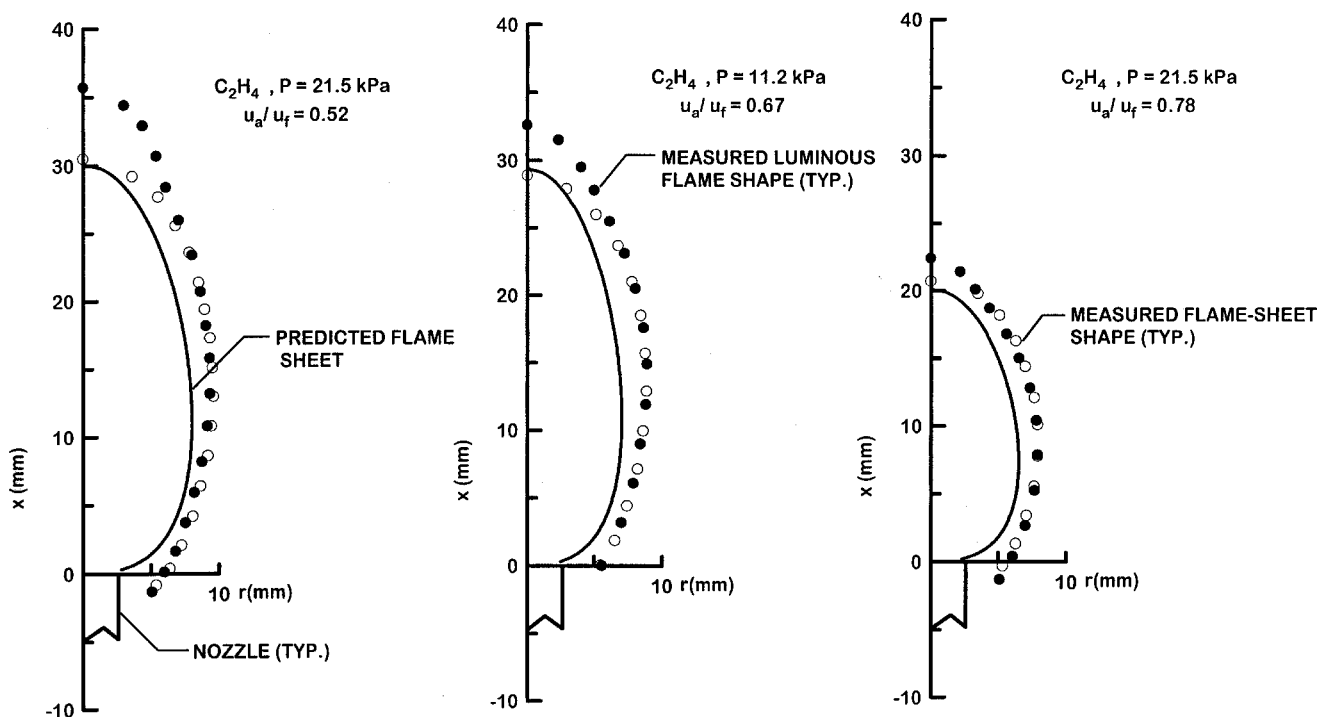

Fig. 7 Measured flame-sheet and luminous-flame shapes for soot-containing ethylene-fueled laminar-jet diffusion flames having a burner diameter of 4.8 mm at various small air coflow velocity ratios.

does not have a significant impact on predictions of flame-sheet location.

Examples of measured and predicted flame-sheet shapes for both soot-free and soot-containing flames involving other fuels, propane/air and acetylene/air flames, having various velocity ratios are illustrated in Figs. 8 and 9. Similar to Fig. 7, results with and without the CH filter are not always the same with the luminous-flame boundary extending beyond the flame sheet because of luminosity

from soot in the fuel-lean portion of the flame in some instances. Only predictions for the flame-sheet shape in still air are shown because these flames are not at laminar smoke-point conditions and have small air/fuel velocity ratios; notably, the comparisons between predicted and measured of flame-sheet shapes are excellent. (Corresponding comparisons between measured and predicted luminous-flame shapes at laminar smoke-point conditions can be found in Lin and Faeth.[9])
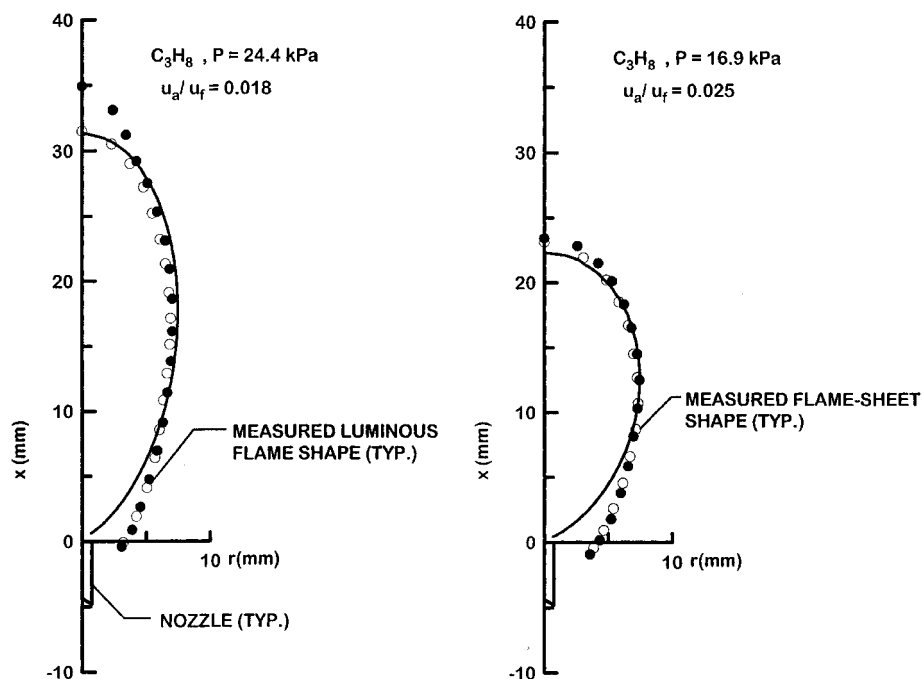
Fig. 8 Measured flame-sheet and luminous-flame shapes and predicted flame-sheet shapes for both soot-containing and soot-free propane-fueled laminar-jet diffusion flames having a burner diameter of 1.6 mm at various small air coflow velocity ratios.
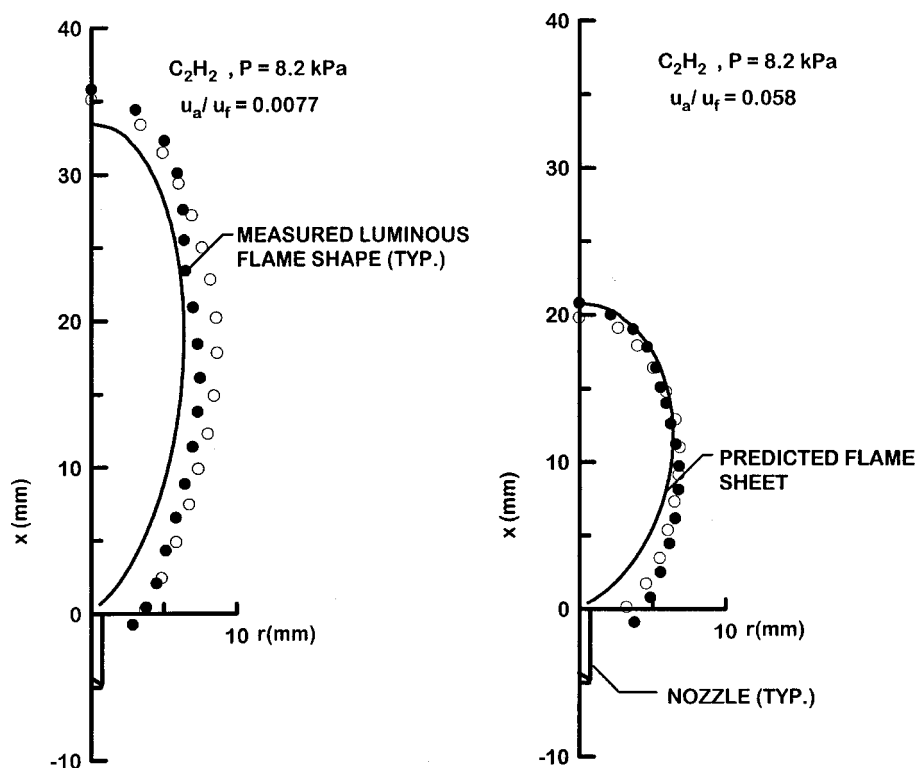

Fig. 9 Measured flame-sheet and luminous-flame shapes and predicted flame-sheet shapes for both soot-containing and soot-free acetylene-fueled laminar-jet diffusion flames having a burner diameter of 1.6 mm at various small coflow velocity ratios.

Conclusions

The luminous flame-sheet and luminous-flame boundaries of steady, nonbuoyant round hydrocarbon-fueled laminar-jet diffusion flames in still and coflowing air were studied both experimentally and theoretically. Present conditions included acetylene-, methane-, propane-, and ethylene-fueled flames having reactant temperatures of 300 K, ambient pressures of 4–50 kPa, jet-exit Reynolds numbers of 3–54, initial air/fuel velocity ratios of 0–9, and luminous flame lengths of 5–55 mm. The present flames involved both soot-free and soot-containing flames but the latter were not emitting soot and generally did not approach laminar smoke-point condi-

tions. Both new and earlier[5,9] measurements were used to evaluate predictions of luminous flame-sheet and luminous-flame boundaries based on extension of simplified analyses from Spalding[2] and Mahalingam et al.[8] The major conclusions of the study are as follows:

1) The present simplified analysis of nonbuoyant laminar-jet diffusion flames in coflow, extended from Mahalingam et al.,[8] provided reasonably good predictions of flame-sheet shapes of both soot-free and soot-emitting flames for $u_{ao}/u_{fo} > 0.5$ and $Fr_a > 1$ after appropriate selection of empirical parameters for the simplified theory summarized in Table 2.

2) The simplified analysis of nonbuoyant laminar-jet diffusion flames in still air from Spalding[2] provided reasonably good predictions of flame-sheet shapes of both soot-free and soot-containing flames in slow-moving coflow for $u_{ao}/u_{fo} < 0.2$ and $Fr_f > 5$ after appropriate selections of empirical parameters for the simplified theory summarized in Table 2.

3) Based on present findings about flame-sheet and luminous-flame boundaries of nonbuoyant laminar-jet diffusion flames in still and coflowing air, flame-sheet and luminous-flame lengths increase linearly with fuel flow rates but are relatively independent of jet-exit diameter, pressure, and air/fuel velocity ratio (for flames in coflow). Finally, flames in still air are roughly 50% longer than flames in reasonably strong coflow ($u_{ao}/u_{fo} > 1$) at comparable conditions.

4) Based on present findings about flame-sheet and luminous-flame boundaries of nonbuoyant laminar-jet diffusion flames in still and coflowing air, characteristic flame-sheet and luminous-flame diameters vary linearly with jet-exit diameter and are relatively independent of flow physical properties and jet-exit Reynolds numbers. For flames having significant coflow levels ($u_{ao}/u_{fo} > 1$), however, the characteristic luminous flame diameters are also proportional to the square root of u_{fo}/u_{ao}.

5) Luminous-flame lengths progressively increased compared to flame-sheet lengths as the laminar smoke point was approached for nonbuoyant laminar-jet diffusion flames in both still and coflowing air. In both cases luminous-flame lengths at the laminar smoke point were roughly twice as long as flame-sheet length as a result of the presence of hot luminous soot particles in the fuel-lean portions of the soot-containing flames.

Limitations of the present findings should be noted, as follows: these results should be used with caution outside the present test range until the results are definitively confirmed for longer-term microgravity conditions where the intrusion of effects of transient flame development and buoyancy are absent (notably, both these effects tend to reduce the luminous flame dimensions[6]); these results were developed for luminous flame shapes and the simplified theories should not be assumed to apply to other important flame structure properties (temperatures, velocities, species concentrations, etc.) where good performance of such simplified methods has not been established and frankly seems unlikely.

Acknowledgments

References

[1]Burke, S. P., and Schumann, T. E. W., "Diffusion Flames," *Industrial and Engineering Chemistry*, Vol. 20, No. 10, 1928, pp. 998–1004.

[2]Spalding, D. B., *Combustion and Mass Transfer*, Pergamon, New York, 1979, pp. 185–195.

[3]Kuo, K. K., *Principles of Combustion*, Wiley, New York, 1986, pp. 360–370.

[4]Sunderland, P. B., Mendelson, B. J., Yuan, Z.-G., and Urban, D. L., "Shapes of Buoyant and Nonbuoyant Laminar Jet Diffusion Flames," *Combustion and Flame*, Vol. 116, No. 3, 1999, pp. 376–386.

[5]Lin, K.-C., Faeth, G. M., Sunderland, P. B., Urban, D. L., and Yuan, Z.-G., "Shapes of Nonbuoyant Round Luminous Hydrocarbon/Air Laminar Jet Diffusion Flames," *Combustion and Flame*, Vol. 116, No. 3, 1998, pp. 415–431.

[6]Urban, D. L., Yuan, Z.-G., Sunderland, P. B., Linteris, G. T., Voss, J. E., Lin, K.-C., Dai, Z., Sun, K., and Faeth, G. M., "Structure and Soot Properties of Nonbuoyant Ethylene/Air Laminar Jet Diffusion Flames," *AIAA Journal*, Vol. 36, No. 8, 1998, pp. 1346–1360.

[7]Williams, F.A., *Combustion Theory*, 2nd ed., Benjamin/Cummings Publishing, Menlo Park, CA, 1985, pp. 38-47.

[8]Mahalingam, S., Ferziger, J. H., and Cantwell, B. I., "Self-Similar Diffusion Flames," *Combustion and Flame*, Vol. 82, No. 2, 1990, pp. 231–234.

[9]Lin, K.-C., and Faeth, G. M., "Shapes of Nonbuoyant Round Luminous Laminar Jet Diffusion Flames in Coflowing Air," *AIAA Journal*, Vol. 37, No. 6, 1999, pp. 759–765.

[10]Hussman, A. W., and Maybach, G. W., "The Film Vaporizer Combustor," *SAE Transactions*, Vol. 69, 1961, pp. 563–574.

[11]Bahr, D. W., "Gas Turbine Engine Emission Abatement—Status and Needed Advancements," *Gas Turbine Combustion Design Problems*, edited by A. H. Lefebvre, Hemisphere, Washington, DC, 1979, pp. 205–223.

[12]Haynes, B. S., and Wagner, H. G., "Soot Formation," *Progress in Energy and Combustion Science*, Vol. 7, No. 4, 1981, pp. 229–273.

[13]Wu, K.-T., and Essenhigh, R. H., "Mapping and Structure of Inverse Diffusion Flames of Methane," *Proceedings of the Combustion Institute*, Vol. 20, Combustion Inst., Pittsburgh, PA, 1984, pp. 1925–1932.

[14]Glassman, I., "Soot Formation in Combustion Processes," *Proceedings of the Combustion Institute*, Vol. 22, Combustion Inst., Pittsburgh, PA, 1988, pp. 295–311.

[15]Sugiyama, G., "Nonluminous Diffusion Flame of Diluted Acetylene in Oxygen Enriched Air," *Proceedings of the Combustion Institute*, Vol. 25, Combustion Inst., Pittsburgh, PA, 1994, pp. 601–608.

[16]Du, J., and Axelbaum, R. L., "The Effect of Flame Structure on Soot-Particle Inception in Diffusion Flames," *Combustion and Flame*, Vol. 100, No. 3, 1995, pp. 367–375.

[17]Lin, K.-C., "Hydrodynamic Effects on Soot Formation in Laminar Hydrocarbon-Fueled Diffusion Flames," Ph.D. Dissertation, Dept. of Aerospace Engineering, Univ. of Michigan, Ann Arbor, MI, June 1996.

[18]Lin, K.-C., and Faeth, G. M., "Hydrodynamic Suppression of Soot Emissions in Laminar Diffusion Flames," *Journal of Propulsion and Power*, Vol. 12, No. 1, 1996, pp. 10–17.

[19]Dai, Z., and Faeth, G. M., "Hydrodynamic Suppression of Soot Formation in Laminar Coflowing Jet Diffusion Flames," *Proceedings of the Combustion Institute*, Vol. 28, Combustion Inst., Pittsburgh, PA, 2000, pp. 2085–2092.

[20]Hamins, A., Gordon, A. S., Saito, K., and Seshadri, K., "Acetone Impurity in Acetylene from Tanks," *Combustion Science and Technology*, Vol. 45, No. 5, 1986, pp. 309, 310.

[21]Braun, W. G., Danner, R. P., and Daubert, T. E., *Technical Data Book—Petroleum Refining*, 3rd ed., American Petroleum Inst., Washington, DC, 1976, Chaps. 11 and 13.

[22]Schug, K. P., Manheimer-Timnat, Y., Yaccarino, P., and Glassman, I., "Sooting Behavior of Gaseous Hydrocarbon Diffusion Flames and the Influence of Additives," *Combustion Science and Technology*, Vol. 22, Nos. 5 and 6, 1980, pp. 235–250.

[23]Gomez, A., Sidebotham, G., and Glassman, I., "Sooting Behavior in Temperature-Controlled Laminar Diffusion Flames," *Combustion and Flame*, Vol. 58, No. 1, 1984, pp. 45–57.

[24]Sunderland, P. B., Mortazavi, S., Faeth, G. M., and Urban, D. L., "Laminar Smoke-Points of Nonbuoyant Jet Diffusion Flames," *Combustion and Flame*, Vol. 96, No. 1, 1994, pp. 97–103.

[25]Urban, D. L., Yuan, Z.-G., Sunderland, P. B., Lin, K.-C., Dai, Z., and Faeth, G. M., "Smoke-Point Properties of Nonbuoyant Round Laminar Diffusion Flames," *Proceedings of the Combustion Institute*, Vol. 28, Combustion Inst., Pittsburgh, PA, 2000, pp. 1965–1972.

J. P. Gore
Associate Editor